A Novel M_8L_6 Cubic Cage That Binds Tetrapyridyl Porphyrins: Cage and Solvent Effects in Cobalt-Porphyrin-Catalyzed Cyclopropanation Reactions

Valentinos Mouarrawis,[a] Eduard O. Bobylev,[a] Bas de Bruin,*[a] and Joost N. H. Reek*[a]

Dedicated to Professor Christian Bruneau.

Abstract: Confinement of a catalyst can have a significant impact on catalytic performance and can lead to otherwise difficult to achieve catalyst properties. Herein, we report the design and synthesis of a novel caged catalyst system **Co–G@Fe$_8$(Zn–L·1)$_6$**, which is soluble in both polar and apolar solvents without the necessity of any post-functionalization. This is a rare example of a metal-coordination cage able to bind catalytically active porphyrins that is soluble in solvents spanning a wide variety of polarity. This system was used to investigate the combined effects of the solvent and the cage on the catalytic performance in the cobalt catalyzed cyclopropanation of styrene, which involves radical intermediates. Kinetic studies show that DMF has a protective influence on the catalyst, slowing down deactivation of both **[Co(TPP)]** and **Co–G@Fe$_8$(Zn–L·1)$_6$**, leading to higher TONs in this solvent. Moreover, DFT studies on the **[Co(TPP)]** catalyst show that the rate determining energy barrier of this radical-type transformation is not influenced by the coordination of DMF. As such, the increased TONs obtained experimentally stem from the stabilizing effect of DMF and are not due to an intrinsic higher activity caused by axial ligand binding to the cobalt center (**[Co(TPP)(L)]**). Remarkably, encapsulation of **Co–G** led to a three times more active catalyst than **[Co(TPP)]** (TOF_{ini}) and a substantially increased TON compared to both **[Co(TPP)]** and free **Co–G**. The increased local concentration of the substrates in the hydrophobic cage compared to the bulk explains the observed higher catalytic activities.

Introduction

Catalysis in confined spaces using self-assembled cages with catalysts is an attractive approach to enhance catalytic performance.[1] Several examples are reported in which cages are used as hosts for catalytically active guests.[2] The encapsulation of a catalyst in a molecular container with a well-defined confined space imposes so-called second coordination sphere effects, which can influence the activity and/or selectivity of a catalytic reaction.[3] The confinement of such guests leads to unprecedented reactivities and selectivities that can be difficult to achieve via ligand modification.[4] However, the development of supramolecular architectures able to bind catalysts is rather challenging and associated with various different encounters: (1) The design of a cage that has sufficient space to accommodate the desired catalytically active guest and and has large enough apertures for substrate access and product release;[5] (2) For any guest to be able to bind inside the cage a complementary and enthalpically favorable host-guest interaction is needed to form the respective inclusion complex;[6] (3) The catalytically active caged catalyst needs to have enough cavity space for a catalytic transformation to occur, as the lack of space may lead to substrate or product inhibition; (4) The solubility of the host-guest complex is typically the solubility of the host and usually leads to solubilizing otherwise insoluble guests in solvents that are favorable in certain catalytic applications;[7] (5) The solubility of metal-coordination cages is generally limited to polar solvents such as water, DMF, DMSO, or acetonitrile and this may limit their application or performance in catalysis where different solvents are desired.

We previously reported a strategy in which a catalytically active cobalt(II) meso-tetra(4-pyridyl)metalloporphyrin (**Co–G**), encapsulated in a M_8L_6 cubic cage, showed higher TON than the non-encapsulated catalyst in the radical-type cyclopropanation of styrene, as confinement reduced the number of unwanted side reactions of reactive radical intermediates.[2d,5] Interestingly, the solvent was found to influence the catalytic efficiency, as the use of acetone/water mixtures instead of acetone drastically increased the TON of the catalyst. Similarly, the performance of the well-established cobalt(II) meso-tetraphenylporphine **[Co(TPP)]** catalyst in radical-type transformations is strongly dependent on the solvent.[8] As such, we decided to develop a caged catalyst system that is soluble in a

[a] *V. Mouarrawis, E. O. Bobylev, Prof. Dr. B. de Bruin, Prof. Dr. J. N. H. Reek*
Homogeneous and Supramolecular Catalysis Group
Van' t Hoff Institute for Molecular Science (HIMS)
University of Amsterdam (UvA), Science Park 904
1098 XH Amsterdam (The Netherlands)
E-mail: b.debruin@uva.nl
J.N.H.Reek@uva.nl

Supporting information for this article is available on the WWW under https://doi.org/10.1002/chem.202100344

wide range of solvents, allowing to study the effects of the solvent in catalysis under confinement conditions. We anticipated that the combined effects of a protective environment of a metal-coordination cage and the use of different solvents can be used to optimize the performance of cobalt(II)-catalyzed radical-type transformations. To date, the majority of metal-coordination cages are positively or negatively charged species, which typically generate insoluble materials in apolar solvents.[9] Herein, we report the synthesis of a novel supramolecular cage that is soluble in a range of solvents and allowed us to investigate the effects of both confinement and solvent on the radical-type cyclopropanation of styrene.

As such we developed a new Nitschke-type cubic M_8L_6 cage compound that efficiently encapsulates tetrapyridyl porphyrins and can be easily exo-functionalized to influence the solubility (Figure 1A). The extension of the porphyrin building block reported by Nitschke (Figure 1D)[10] by one phenyl group (Figure 1B) leads to the formation of a larger analog that has sufficient space to encapsulate a catalytically active porphyrin complex. The aperture of the cage is large enough to allow substrates to enter and products to exit from the cage (Figure 1A).

Results and Discussion

We started our investigation with the synthesis of a novel supramolecular cage that is soluble in both polar and apolar solvents. The extended porphyrin building block **Zn**–**L** was efficiently synthesized from 5,10,15,20-(tetra-4-bromophenyl) porphyrin in two steps and overall yield of 85% (see Supporting Information).

The reaction between subcomponent **Zn**–**L** (6 equiv.), 5-(icosyloxy)picolinaldehyde (**1**, 24 equiv.) and iron(II) triflate (8 equiv.) in DMF at 70 °C resulted in the formation of a new species via imine bond formation (Figure 2A). Typical shifts in the ^{1}H NMR spectra are in line with the formation of a highly symmetrical species containing low spin tris(pyridyl-imine) iron (II) moieties. ^{1}H NMR diffusion-ordered spectroscopy (DOSY) confirms the formation of a single species in solution that is much larger than the components (Figure 2B). Based on the diffusion constant the diameter of the self-assembled structure is 45 Å, which is in line with the formation of the desired cubic cage (Fe_8(**Zn**–**L**·**1**)$_6$). Additional proof for the formation of the cage was provided by high resolution electrospray mass spectrometry (HR-ESI-MS), which shows various peaks associ-

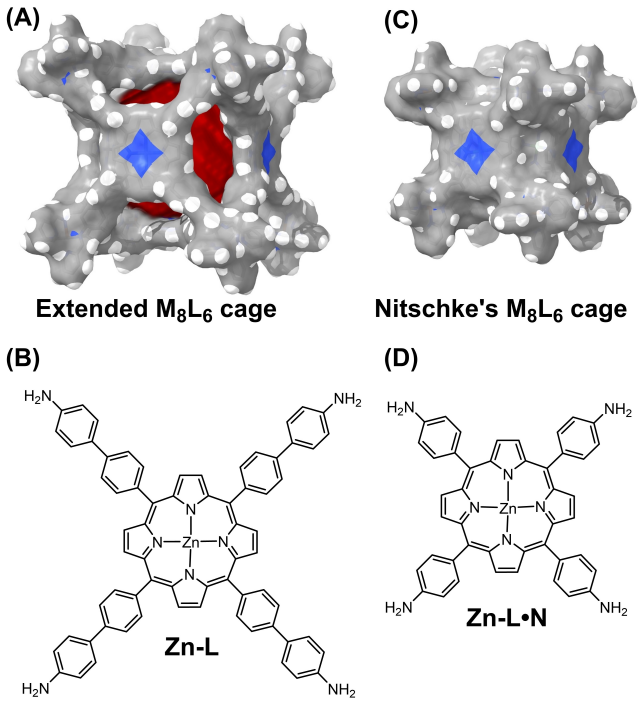

Figure 1. (A) Molecular model of the extended M_8L_6 cubic cage (the icosyl chains are omitted). (B) The extended porphyrin building block (**Zn**–**L**) used in the self-assembly process. (C) The reported crystal structure of Nitschke's M_8L_6 cage and (D) the corresponding building block (**Zn**–**L**·**N**).

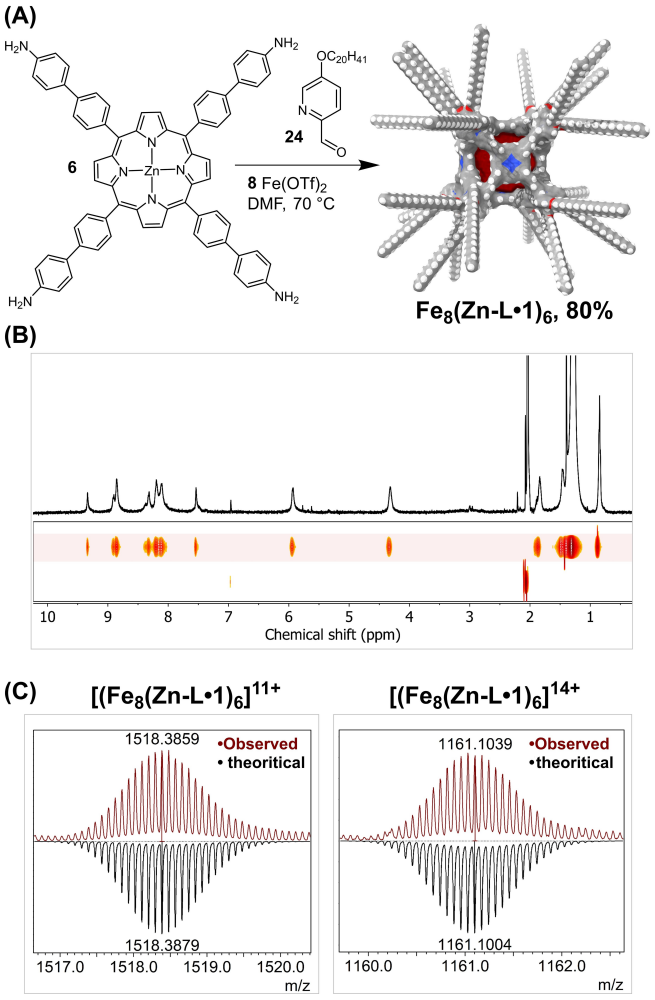

Figure 2. (A) Synthetic procedure of Fe_8(**Zn**–**L**·**1**)$_6$ and geometry optimized structure of Fe_8(**Zn**–**L**·**1**)$_6$ using a semi-empirical extended tight-binding method (GFN2-xTB).[12] Calculated inner cavity volume of Fe_8(**Zn**–**L**·**1**)$_6$ displayed in red, using Voss Volume Voxelator. (B) ^{1}H-DOSY NMR of Fe_8(**Zn**–**L**·**1**)$_6$ showing a diffusion constant of $3.1 \cdot 10^{-6}$ cm^{2}s^{-1}. (C) Obtained (red) and calculated (black) HR-ESI-MS for the 11^+ (left) and 14^+ (right) species of Fe_8(**Zn**–**L**·**1**)$_6$.

ated to the cubic cage ($Fe_8(Zn–L\cdot 1)_6$) with different charges, in line with the formation of the desired multicationic species (Figure 2C). Our efforts to grow single crystals suitable for X-ray diffraction were unsuccessful (solvent layering and vapor diffusion at different temperatures only led to solid powders, not suitable for analysis via X-ray diffraction). As anticipated, the presence of 24 icosyl groups rendered $Fe_8(Zn–L\cdot 1)_6$ soluble in a wide range of solvents. Although, cage $Fe_8(Zn–L\cdot 1)_6$ is a 16^+ charged species, the presence of hydrophobic tails generated a cage soluble in both apolar (dichloromethane, toluene, and dichloromethane/hexane mixtures) and polar (dimethylformamide, acetone, tetrahydrofuran) solvents. This is the first example where a metal-coordination cage is soluble in such a wide range of solvents without any post modifications (i.e. counterion exchange).[7b,11]

Molecular modeling studies were performed to calculate the volume of the central cavity. As a starting point, the crystal structure reported for the smaller analog by the group of Nitschke was used[10] to generate the new coordinates, and the geometry of the cage was optimized with GFN2-xTB.[12] Thus obtained models revealed that the Zn-tetrapyridyl porphyrin (**Zn–G**) has an outer molecular volume of ~572 Å^3, and the empty cage $Fe_8(Zn–L\cdot 1)_6$ has a volume of ~3300 Å^3. Combined with the Zn–Zn distance of 19 Å between the opposite faces of the cubic cage, the cavity size is optimal to bind **Zn–G**. Furthermore, we anticipated that the tetratopic zinc-pyridyl coordination provides optimal multivalent (tetratopic) binding resulting in a high binding affinity of the symmetrical tetrapyridine-porphyrin guest **Zn–G**.

When a DMF solution of pre-formed $Fe_8(Zn–L\cdot 1)_6$ was stirred overnight in the presence of **Zn–G**, there was no indication of a new species, as NMR and MS revealed only the empty cage. The one-pot reaction of **Zn–G** with **Zn–L**, **1**, and iron(II) triflate in the correct stoichiometric ratios led to the disappearance of the ^{1}H NMR peaks of the free **Zn–G** and three new, strongly upfield shifted guest peaks appeared at 6.4, 5.6 and 2.54 ppm (Figure 3B) indicating molecular confinement of **Zn–G**. Signals of the cage wall split in a 4:2 ratio upon encapsulation of **Zn–G**. The observed $\Delta\delta$ values of **Zn–G** upon encapsulation are consistent with previous encapsulation studies of **Zn–G** in similar cubic self-assemble cages.[2d,5,13] DOSY reveals the same diffusion with $Fe_8(Zn–L\cdot 1)_6$ for all signals including the upfield NMR signals that are from protons of the **Zn–G**, indicating the formation of a species with the same size in solution but now with the guest included (Figure 3B). The HR-ESI-MS spectra show peaks that can only be associated to a structure in which one molecule of **Zn–G** is included in the host $Fe_8(Zn–L\cdot 1)_6$. Importantly, no other masses were observed with different stoichiometries of host and guest, in line with the binding of the guest inside the molecular cube (see Supporting Information).

Convinced by the successful synthesis and characterization of the diamagnetic host-guest complex **Zn–G@**$Fe_8(Zn–L\cdot 1)_6$, we next decided to study the encapsulation of catalytically

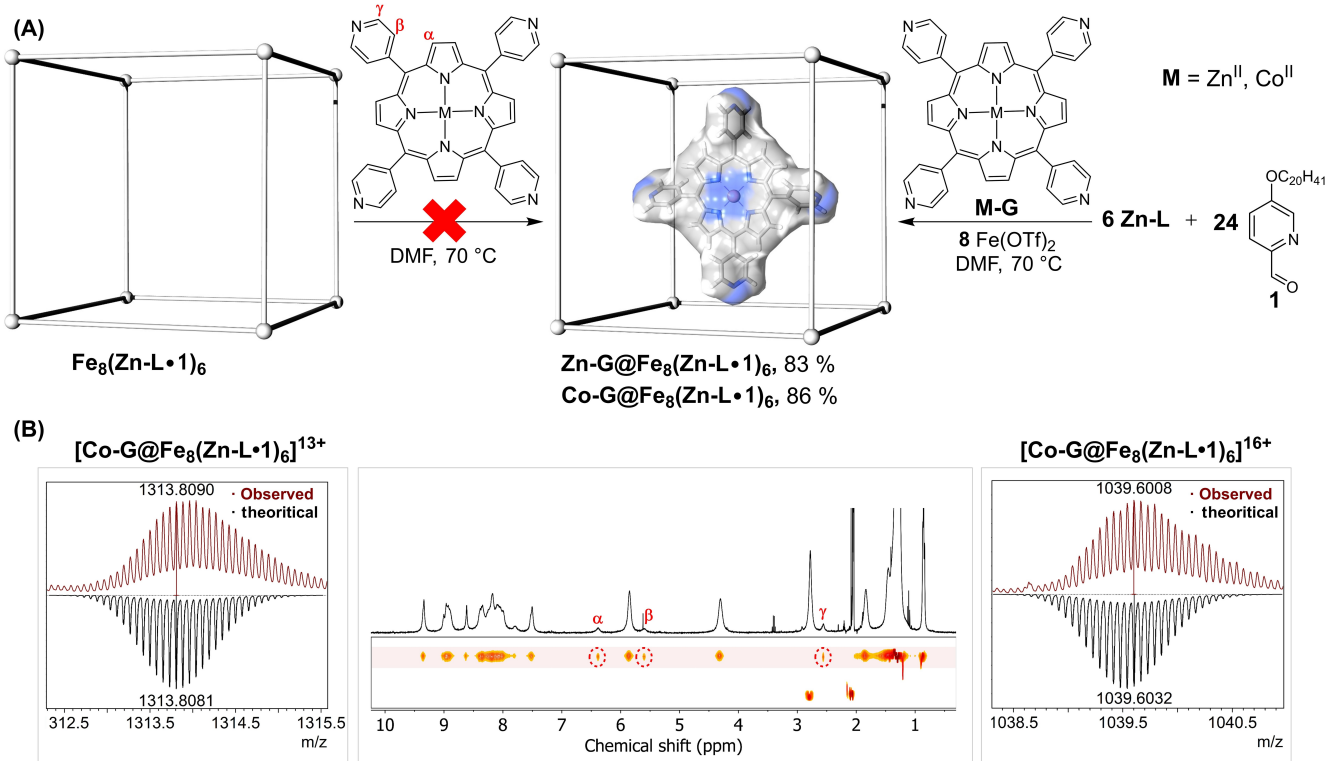

Figure 3. (A) Unsuccessful encapsulation of **M–G** (M=Zn, Co) in $Fe_8(Zn–L\cdot 1)_6$ (left) and one-step synthesis of **M–G@**$Fe_8(Zn–L\cdot 1)_6$, (right). (B) Obtained (red) and calculated (black) HR-ESI-MS for the 13^+ (left) and 16^+ (right) species of **Co–G@**$Fe_8(Zn–L\cdot 1)_6$. ^{1}H-DOSY (middle) of **Zn–G@**$Fe_8(Zn–L\cdot 1)_6$ showing a diffusion constant of $3\cdot 10^{-6}$ cm^2 s^{-1}. Guest peaks are indicated with a circle.

active and paramagnetic cobalt(II)-tetra(4-pyridyl)porphyrin (**Co–G**) via the same approach. The caged-catalyst (**Co–G@Fe$_8$(Zn–L·1)$_6$**) was characterized by HR-ESI-MS (Figure 3B), and the spectra show signals for [(Co–G@Fe$_8$ (Zn–L·1)$_6$) (OTF)$_{16}$–x(OTF)]$^{x+}$ (x = 7–15) associated to the structure with the correct elemental composition. Moreover, the EPR spectrum of **Co–G@Fe$_8$(Zn–L·1)$_6$** in frozen toluene:DMF mixture (100:1) reveals a typical signal for an isolated $S = {}^1/_2$ Co^{II}(por) species with clearly resolved cobalt hyperfine couplings (see Supporting Information). In contrast the EPR signal of free, non-encapsulated **Co–G** is very broad and does not show any hyperfine couplings due to self-aggregation.[2d] Encapsulation of **Co–G** within the cage assembly leads to much sharper signals because the protective environment of the cage prevents self-aggregation. Interestingly, the formation of **Zn–G@Fe$_8$(Zn–L·1)$_6$** and **Co–G@Fe$_8$(Zn–L·1)$_6$** shows that our strategy to accommodate metalloporphyrins in the new cage is applicable to different metals (Zn and Co).

Having established the preparation of a cage containing a cobalt porphyrin **Co–G**, which is soluble in polar and apolar solvents, we decided to first investigate the solvent effects on the cyclopropanation of styrene, by utilizing the well-established **[Co(TPP)]** catalyst for radical-type cyclopropanation reactions. Previous studies included the use of solvents such as benzene, toluene, or chlorobenzene,[8a,14] but we felt that studying the effect of the reaction medium in more detail using separate experiments was needed before studying the effect of the cage in different solvents. Importantly, radical-type transformations involve highly reactive intermediates that can react with the solvent (i.e. via hydrogen atom abstraction),[15] leading to deactivation pathways. Thus, bond dissociation energies (BDEs) can perhaps provide information to selection the solvent. We hypothesized that the use of toluene (BDE of 90 kcal mol^{-1})[16] or DCM (BDE of 96 kcal mol^{-1})[17] may result in a higher stability of the catalyst, as unfavorable reactions of the solvent with the carbene intermediate leading to the formation of catalytically inactive species via HAT can perhaps be suppressed.[18] A series of catalytic experiments were performed to study the effect of the solvent on this reaction by utilizing **[Co(TPP)]** at 0.25 mol% catalyst loading (Table 1).

The reactions were run at 40 °C for 30 h after which the conversion and yields of the product **P1** and side product **P2** were determined by ^{1}H NMR. Surprisingly, DMF (BDE of 82 kcal mol^{-1})[19] was found to be a compatible solvent for the cyclopropanation of styrene, affording the desired product in high yield (70%, TON = 284, Table 1, entry 1). When the reaction was carried out in toluene, the obtained yield was much lower after 30 h reaction time (40%, TON = 164, Table 1, entry 3). When the reaction was carried out in DCM, which is the most stable solvent in terms of BDEs, the product **P1** was formed only in 11% yield (TON = 48, Table 1, entry 2). The positive effect of DMF on the cyclopropanation of **S1** was demonstrated by performing the reaction in 100:1 toluene/DMF mixture, leading to almost the same yield as the reaction carried out in pure DMF (69%, TON = 280, Table 1, entry 4). In all these experiments styrene was present in excess with respect to ethyl diazoacetate. If, however, a 2-fold excess of **S2** (ethyl diazoacetate) was used under the same conditions, an enhanced yield of dimerization product **1** was obtained (5% vs 1%). This stems from the selectivity of this reaction that is determined after the formation of the cobalt-carbene radical intermediate,[20] as the reaction with styrene leads to cyclopropane **P1**, whereas the reaction with a second equivalent of **S2** leads to dimerization.

The differences in yield after 30 h reaction time under the different conditions (Table 1) can be a result of differences in reaction rate, incubation time and stability of the catalyst systems. To distinguish between the different effects we monitored the reaction in various solvents over time. From these studies (Figure 4) it is clear that the initial TOFs in DMF, toluene, and a toluene:DMF mixture (100:1) are similar, thus suggesting that the solvent has little to no influence on the (initial) activity of the catalyst (see also Figure S49 in the supporting information for a zoom of the initial stage of the reaction). However, monitoring the reaction over a longer period reveals that the catalyst deactivates much quicker in toluene than in DMF or in a 100:1 toluene:DMF mixture (Figure 4A).

Next, density functional theory (DFT-D3, BP86, def2-TZVP) calculations were performed to obtain more insight into the role of DMF on the cobalt-catalyzed cyclopropanation of styrene (Figure 5). In our previous studies, we reported the free energy reaction profile of cobalt-porphyrin catalyzed cyclopropanation of styrene with EDA, in which the rate-determining

Table 1. The solvent effect in [**Co(TPP)**]-catalyzed cyclopropanation of styrene.[a,b]

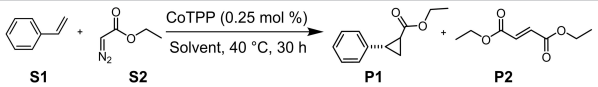

Entry	Solvent	Conversion [%]	P1 [%]	P2 [%]	TON[e]
1	DMF	71	70	1	284
2	DCM	12	11	1	48
3	Toluene	41	40	1	164
4[c]	Toluene: DMF	70	69	1	280
5[d]	DMF	35	30	5	140

[a] Reaction conditions: Catalyst (0.25 mol%) with respect to ethyl diazoacetate (**S2**, 0.32 mmol) and styrene (**S1**, 0.64 mmol) in solvent (1 ml), 40 °C, 30 h under N_2 atmosphere. [b] Conversion of **S2** and yields with respect to **S2** were determined by NMR spectroscopy, using 1,3,5-trimethoxybenzene as internal standard, and averaged from three measurements. [c] Toluene: DMF (100:1). [d] 2-fold excess of **S2** vs **S1**. The conversion and the yields were determined with respect to styrene. [e] Turnover number (TON) was determined by dividing the conversion through the catalyst loading (conv/0.25).

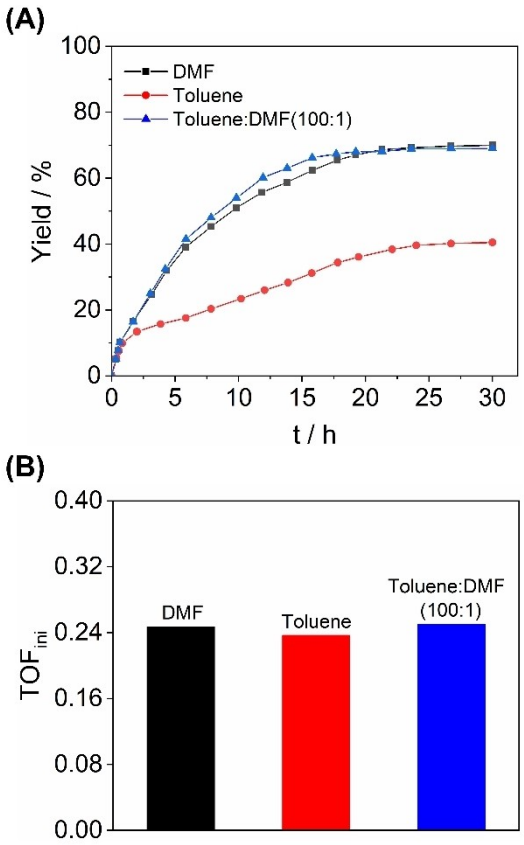

Figure 4. (A) Reaction profile of **[Co(TPP)]** in the cyclopropanation of styrene at 0.25 mol% catalyst loading in DMF (black), toluene (red), toluene:DMF (100:1, blue). (B) Plot of TOF_{ini} calculated at 10% conversion in different solvents.

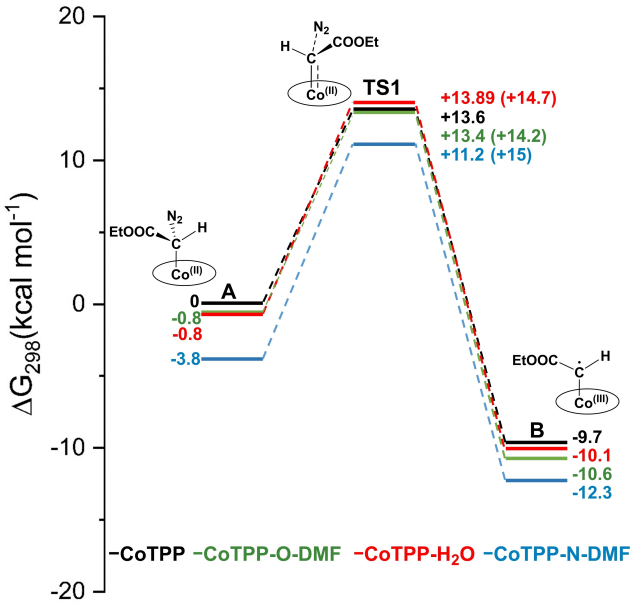

Figure 5. Free energy changes for the rate-determining step in the cyclopropanation of styrene with EDA using **[Co(TPP)]**, **[Co(TPP)(-O-DMF)]**, **[Co(TPP)(-N-DMF)]** and **[Co(TPP)(-H_2O)]**. All energies are relative to **A** (**[Co(TPP)]** or **[Co(TPP)(L)]**. The activation energies for **TS1** are reported between parenthesis.

step was found to be the formation of the cobalt-carbene intermediate (TS = +13.6 kcal mol^{-1}).[20,21] We, therefore, re-examined computationally the formation of the carbene-radical species upon axial DMF (O- and N-coordination) and water coordination (Figure 5). If anything, axial ligand coordination was found to lead to (somewhat) higher instead of lower barriers, and the effects are very small for DMF. Interestingly, these results differ from the results obtained by Yamada and co-workers, who showed that in the cobalt(II)-mediated cyclopropanation of olefins using an optically active aldiminato complex the addition of an axial N- or O-donor ligand has a positive effect on the catalytic efficiencies in terms of selectivity and activity.[22] On the basis of a computational follow-up study, they showed that for that catalyst the energy barrier for the formation of the cobalt-carbene intermediate is lowered upon axial ligand coordination.[23]

The DFT calculation clearly confirm that the improved TONs in the presence of DMF are not due to a higher activity caused by N- or O- coordination. These results, combined with the experimental reaction profile, suggest that instead the presence of DMF slows down catalyst deactivation, even with a minor amount of DMF. DMF clearly has a stabilizing effect, and as a result, higher yields of cyclopropane are obtained. While interesting and noteworthy, the exact mechanistic explanation is outside the scope of this work, and is under current investigation in a follow up study.

Next, we decided to investigate the effect of the combined solvent and second coordination sphere effects on the activity of the supramolecular **Co–G@Fe_8(Zn–L·1)$_6$** catalyst. First, we conducted a series of control experiments and optimization of reaction conditions that are summarized in Table 2.

Importantly, **Fe_8(Zn–L·1)$_6$** and **Zn–G@Fe_8(Zn–L·1)$_6$** are not catalytically active, as performing the reaction at 40 or 65 °C did not yield any product (Table 2, entries 1–4). Performing the reaction with **Co–G@Fe_8(Zn–L·1)$_6$** at 40 °C led to 90% conversion, whereas at 65 °C the conversion was similar (Table 2, entries 5 and 6) but led to a higher amount of **P2** (14% vs 17%). Interestingly, the addition of **S2** after stirring **S1** and the supramolecular catalyst for 30 min resulted in higher conversion and lower dimerization of **S2** (Table 2, entry 7). Compared to **[Co(TPP)]**, the caged catalyst gives rise to higher conversions and higher cyclopropane yields, but also leads to a higher amount of dimer product **P2** (Table 2, entries 7 and 8).

With the optimized reaction conditions, the catalytic performance for the caged-catalyst **Co–G@Fe_8(Zn–L·1)$_6$** was studied in different solvents, focusing on differences in stability, activity, and selectivity. Table 3 shows the catalytic results for the cyclopropanation of **S1** in the solvents used for **[Co(TPP)]** (vide supra). The activity of **Co–G@Fe_8(Zn–L·1)$_6$** is substantially higher than the free catalyst (**Co–G**). We infer that encapsulation of **Co–G** sterically protects the cobalt-porphyrin catalyst from pyridine-cobalt coordination, and therefore hinders self-deactivation by blockage of the catalytic cobalt center. For this reason, we focused on comparing the catalytic performance of **Co–G@Fe_8(Zn–L·1)$_6$** with **[Co(TPP)]**, in which self-aggregation is much less profound. When **Co–G@Fe_8(Zn–L·1)$_6$** was used as the catalyst the conversion in toluene was lower (TON = 32,

Table 2. Control experiments and optimization of the reaction conditions for the cyclopropanation of styrene in cages.[a,b]

Entry	Catalyst	T [°C]	Conversion [%]	P1 [%]	P2 [%]
1	Fe_8 (Zn–L·1)$_6$	40	–	–	–
2	Fe_8(Zn–L·1)$_6$	65	–	–	–
3	Zn–G@Fe_8(Zn–L·1)$_6$	40	–	–	–
4	Zn–G@Fe_8(Zn–L·1)$_6$	65	–	–	–
5	Co–G@Fe_8(Zn–L·1)$_6$	40	90	76	14
6	Co–G@Fe_8(Zn–L·1)$_6$	65	95	78	17
7[c]	**Co–G@Fe_8(Zn–L·1)$_6$**	**40**	**96**	**84**	**12**
8	[Co(TPP)]	40	71	70	1

[a] Reaction conditions: Catalyst (0.25 mol%) with respect to **S2**, Styrene (**S1**, 0.16 mmol), ethyl diazoacetate (**S2**, 0.08 mmol) in DMF-d_7 (1 ml), 30 h under N_2 atmosphere. [b] Conversion of **S2** and yields with respect to **S2** were determined by ^{1}H NMR spectroscopy, using 1,3,5-trimethoxybenzene as internal standard. [c] The reaction mixture was stirred for 30 min prior to addition of **S2**.

Table 3. The solvent effect in **Co–G@Fe_8(Zn–L·1)$_6$**-catalyzed cyclopropanation of styrene.[a,b]

Entry	Catalyst	Solvent	Conversion [%]	P1 [%]	P2 [%]	TON[e]
1	**Co–G@Fe8(Zn–L·1)$_6$**	**DMF**	**96**	**84**	**12**	**384**
2	Co–G@Fe8(Zn–L·1)$_6$	DCM	20	18	2	80
3	Co–G@Fe8(Zn–L·1)$_6$	Toluene	8	7	1	32
4[c]	Co–G@Fe8(Zn–L·1)$_6$	Toluene:DMF	33	28	5	132
5	Co–G	DMF	5	3	2	20
6[d]	Co–G@Fe8(Zn–L·1)$_6$	DMF	65	39	26	260

[a] Reaction conditions: Catalyst (0.25 mol%) with respect to **S2**, ethyl diazoacetate (**S2**, 0.32 mmol) and styrene (**S1**, 0.64 mmol) in solvent (1 ml), 40 °C, 30 h under N_2 atmosphere. [b] Conversion of **S2** and yields with respect to **S2** were determined by NMR spectroscopy, using 1,3,5-trimethoxybenzene as internal standard, and averaged from three measurements. [c] Toluene: DMF (100:1). [d] 2-fold excess of **S2**. [e] Turnover number (TON) was determined by dividing the conversion through the catalyst loading (conv/0.25).

Table 3, entry 3) compared to **[Co(TPP)]** (TON = 164, Table 1, entry 3). This is most likely due to the formation of aggregates of the cage catalyst in solution, which leads to diffusion limitation for substrate enter and product exit. When the diamagnetic **Zn–G@Fe_8(Zn–L·1)$_6$** was dissolved in toluene-d_8 in the same concentration as the catalytic process a gel-like solution was formed and the corresponding ^{1}H-NMR signals of the cage became very broad (see Supporting Information).[24] The reaction in toluene/DMF mixture (100:1), resulted in increased conversion due to less aggregation of **Co–G@Fe_8(Zn–L·1)$_6$** in solution (TON = 132, Table 3, entry 4), as evidenced by the lower viscosity of the solution and the less broad ^{1}H-NMR of the diamagnetic analog (**Zn–G@Fe_8(Zn–L·1)$_6$**). The reaction in DCM led to the formation of **P1** and **P2** in 18% and 2% yield, respectively (TON = 80, Table 3, entry 2). The use of **Co–G@Fe_8(Zn–L·1)$_6$** in DMF efficiently facilitated the cyclopropanation and converts the substrates to **P1** and **P2** in 84% and 12% yield (TON = 384, Table 3, entry 1).

Remarkably, the encapsulated catalyst increased the conversion by 25%, outperforming both **[Co(TPP)]** and **Co–G**. Although the confined catalyst enhances dimerization of **S2**, the yield of **P1** was 14% higher than with **[Co(TPP)]**. Pure DMF is clearly the optimal solvent for cyclopropanation with both **Co–G@Fe_8(Zn–L·1)$_6$** and **[Co(TPP)]**. Interestingly however, the use of small amounts of DMF in toluene has a smaller beneficial effect on the TONs of **Co–G@Fe_8(Zn–L·1)$_6$** (Table 3, entries 3–4) than was observed for **[Co(TPP)]** (Table 1, entries 3–4). We ascribe this to complete and incomplete breakdown of aggregates of **Co–G@Fe_8(Zn–L·1)$_6$** in pure DMF and in 100:1 toluene:DMF mixtures, respectively. A lower effective concentration of DMF in the hydrophobic interior of the caged catalyst leading to less efficient protection of the catalyst by DMF from deactivation cannot be fully excluded though.

To gain more insight on the cage effect on catalysis, the reaction was monitored over time by ^{1}H NMR spectroscopy, from which the kinetic profiles in DMF for **[Co(TPP)]** and **Co–G@Fe_8(Zn–L·1)$_6$** were obtained (Figure 6A and B). As the environment of the caged-catalyst differs from the bulk solution, different kinetics are expected relative to the free **[Co(TPP)]** catalyst. Interestingly, **Co–G@Fe_8(Zn–L·1)$_6$** exhibits a higher activity compared to **[Co(TPP)]**, which is accompanied by higher dimerization of **S2**. We ascribe both effects to accumulation of substrate in the hydrophobic cage, thus leading to a higher local substrate concentration than in the bulk, and therefore the reaction rates for both cyclopropanation and carbene dimerization are enhanced. The accumulation of substrate is supported by the increased formation of dimer **P2**, as a result of the initial higher concentration of the diazo compound compared to styrene.

As shown in Table 1 (entry 1), dimerization with **[Co(TPP)]** is negligible, whereas **Co–G@Fe_8(Zn–L·1)$_6$** forms a relatively higher amount of dimer (Table 3, entry 1). Additionally, the reaction profile of **Co–G@Fe_8(Zn–L·1)$_6$** in the first 10 minutes reveals the concurrent formation of dimer and cyclopropane, which is followed by the exclusive formation of **P1**, as **P2** formation is suppressed by the decreasing concentration of **S2**. Importantly, the confined catalyst reached a TON of 384, outperforming **[Co(TPP)]** (TON = 284) and **Co–G** (TON = 20) in the cobalt-mediated cyclopropanation of styrene (Figure 6C)

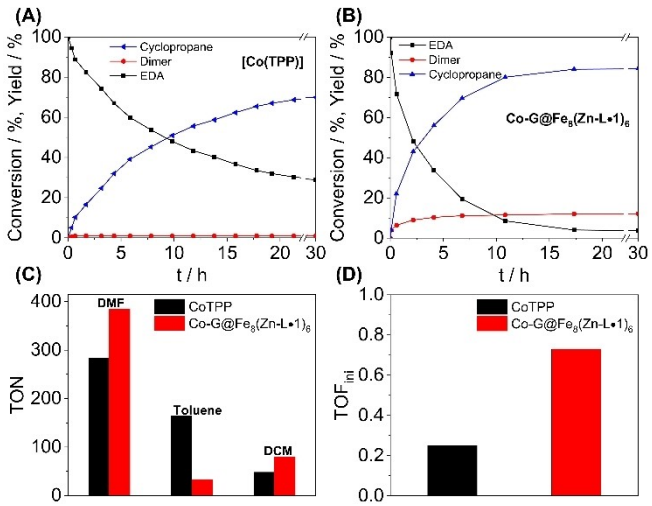

Figure 6. (A) Reaction profile of **[Co(TPP)]** and (B) **Co–G@Fe$_8$(Zn–L·1)$_6$** in the cyclopropanation of styrene at 0.25% catalyst loading. (C) TON for **[Co(TPP)]** and **Co–G@Fe$_8$(Zn–L·1)$_6$** in different solvents. (D) Plot of TOF$_{ini}$ for the formation of **P1** calculated at 10% conversion. Data is obtained by fitting the initial part of the reaction rate curve of **Co–G@Fe$_8$(Zn–L·1)$_6$** and **[Co(TPP)]** (see Supporting Information).

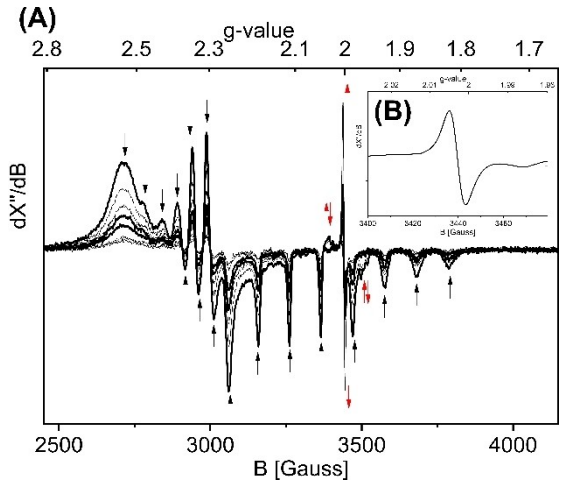

Figure 7. (A) EPR spectra of **Co–G@Fe$_8$(Zn–L·1)$_6$** after adding ethyl diazoacetate (40 equiv.) in frozen toluene:DMF mixture (100:1) at 20 K followed in time upon thawing and refreezing (microwave frequency: 9.357052 GHz; microwave power 0.63 mW; modulation amplitude: 4 Gauss). (B) Zoomed part showing the organic radical.

and the initial TOF of the caged catalyst **Co–G@Fe$_8$ (Zn–L·1)$_6$** is nearly 3 times higher than that of **[Co(TPP)]** (Figure 6D). These results clearly show that encapsulation of **Co–G** renders the catalyst with a higher activity than both free **Co–G** and **[Co(TPP)]**.

Next, we explored the alkene substrate scope of the cyclopropanation reaction by the caged catalyst in order to investigate whether the enhanced catalytic performance of the **Co–G@Fe$_8$(Zn–L·1)$_6$** compared to **[Co(TPP)]** is substrate dependent. We started our investigations testing 4-methoxy styrene. As anticipated the use of a styrene with an electron donating-group led to increased yields for cyclopropane and dimer formation when **Co–G@Fe$_8$(Zn–L·1)$_6$** was used (see Supporting Information, Table S4, entries 1 and 2). Styrenes with electron-withdrawing substituents also proved to be formed in higher yields when the caged catalyst was used (see Supporting Information, Table S4, entries 3–6). Similarly, the use of an electron-deficient alkene such as ethyl acrylate resulted in 22% higher EDA conversion when using **Co–G@Fe$_8$(Zn–L·1)$_6$** instead of **[Co(TPP)]** as the catalyst (see Supporting Information, Table S4, entries 7 and 8). Interestingly, the use of simple olefins such as 1-hexene gave the corresponding cyclopropane in low yields with minor enhancement (9% vs 5%) when the caged catalyst was used (see Supporting Information, Table S4, entry 8 and 9).

As the environment of the caged-catalyst differs from the bulk solution, we were interested to explore the possibility to detect the elusive Co-carbene species embedded in the protective cage. We therefore followed the reaction of the caged catalyst (**Co–G@Fe$_8$(Zn–L·1)$_6$**) with EDA by EPR spectroscopy, measured in frozen toluene:DMF mixtures (100:1). Addition of 40 equiv. of EDA to the solution of **Co–G@Fe$_8$(Zn–L·1)$_6$** at RT resulted in a considerable decrease in intensity of the S=$^1/_2$ Co^{II}(por) species (Figure 7A) in the caged catalyst (**Co–G@Fe$_8$(Zn–L·1$_6$)**) (measured at 20 K), and the initial formation of a weak signal (Figure 7A-i) with *g*-values of a species that are in the range of previously characterized terminal carbene species (Co^{II}-(Cor)(CHCOOEt)[25] and [Co^{II}(3,5-Di-^{t}BuChenPhyrin)-(CHCOOEt)][20]). Interestingly, the stability of the detected Co-carbene radical species embedded in the cage is higher than with **[Co(TPP)]**, as previous attempts to characterize the **[Co(TPP)]**-carbene were unsuccessful (EPR silence). Following the reaction of **Co–G@Fe$_8$(Zn–L·1)$_6$** with excess EDA over time, by repeated thawing/warming and refreezing of the EPR tube, led to the gradual disappearance of the EPR signals of (**Co–G@Fe$_8$(Zn–L·1$_6$)**), appearance and disappearance of the carbene radical signals and appearance of an EPR signal without any hyperfine couplings indicating the formation of a free organic radical presumably trapped in the supramolecular cage (Figure 7B-ii). Interestingly, signals corresponding to a "bridging carbene" species (see Figure S47, supporting information), as reported previously for [Co^{II}(3,5-Di-^{t}BuChenPhyrin)(CHCOOEt)], were not observed. Presumably, formation of such a "bridging carbene" is disfavored by the molecular confinement inside the cage, and formation of such species would probably lead to a distorted [Co^{II}(por)] system that does not bind properly inside the **Fe$_8$(Zn–L·1)$_6$** cage. Overlap of the resulting signals of a "bridging carbene" in low(er) concentrations with the signals stemming from **Co–G@Fe$_8$(Zn–L·1)$_6$** cannot be fully excluded though.

Conclusions

To summarize, we have developed a novel and catalytically active caged-system **Co–G@Fe$_8$(Zn–L·1)$_6$**, soluble in both polar and apolar solvents without the necessity of any post-

functionalization. The icosyl functionalization method developed herein may well also allow other Nitschke-type cages to be solubilized in various solvents to expand their reach of desired applications. This is a rare example of a large cage able to encapsulate catalytically active porphyrins soluble in several solvents of different polarity. The synthesis is based on the self-assembly of subcomponents **1** and **Zn**–**L** in which the catalyst acts as a template for the formation of an octahedral iron-iminopyridine coordination complex. Moreover, we demonstrate that DMF has a protective influence on the catalysts, slowing down deactivation of both **[Co(TPP)]** and **Co**–**G@Fe$_8$(Zn**–**L**·**1)$_6$** during radical-cyclopropanation of styrene. DFT studies reveal similar energy barriers for the rate-determining step of this reaction for **[Co(TPP)]** and **[Co(TPP)(L)]**, with DMF acting as an axial ligand L, thus showing that the observed higher TONs in DMF are not due to an intrinsic higher activity caused by axial ligand binding. Kinetic studies confirm that initial rates in toluene and DMF are similar, but that catalyst deactivation is faster in toluene than in DMF or toluene:DMF (100 : 1) mixtures. The combined effects of the solvent and the cage on the activity and stability of the **Co**–**G@Fe$_8$(Zn**–**L**·**1)$_6$** catalyst were investigated. Interestingly, encapsulation of **Co**–**G** led to a three times more active catalyst than **[Co(TPP)]** (TOF_{ini}) and a substantially increased TON compared to both **[Co(TPP)]** and free **Co**–**G**. The enhanced performance of the catalyst upon encapsulation demonstrates the effect of the cage. We infer that the increased local concentration of ethyl diazoacetate and styrene in the cage compared to the bulk leads to higher catalytic activities.

Acknowledgements

Financial support from The Netherlands Organization for Scientific Research (NWO TOP-PUNT) and the University of Amsterdam (Research Priority Area Sustainable Chemistry) is gratefully acknowledged.

Conflict of Interest

The authors declare no conflict of interest.

Keywords: Confinement · cyclopropanation · homogeneous catalysis · self-assemble cages · solvent effect

[1] a) M. Morimoto, S. M. Bierschenk, K. T. Xia, R. G. Bergman, K. N. Raymond, F. D. Toste, *Nat. Can.* **2020**, *3*, 969–984; b) Q. Zhang, L. Catti, K. Tiefenbacher, *Acc. Chem. Res.* **2018**, *51*, 2107–2114; c) M. Yoshizawa, J. K. Klosterman, M. Fujita, *Angew. Chem. Int. Ed.* **2009**, *48*, 3418–3438; *Angew. Chem.* **2009**, *121*, 3470–3490; d) L. Catti, Q. Zhang, K. Tiefenbacher, *Chem. Eur. J.* **2016**, *22*, 9060–9066; e) Y. Fang, J. A. Powell, E. Li, Q. Wang, Z. Perry, A. Kirchon, X. Yang, Z. Xiao, C. Zhu, L. Zhang, F. Huang, H. C. Zhou, *Chem. Soc. Rev.* **2019**, *48*, 4707–4730.

[2] a) C. García-Simón, R. Gramage-Doria, S. Raoufmoghaddam, T. Parella, M. Costas, X. Ribas, J. N. H. Reek, *J. Am. Chem. Soc.* **2015**, *137*, 2680–2687; b) D. M. Kaphan, M. D. Levin, R. G. Bergman, K. N. Raymond, F. D. Toste, *Science* **2015**, *350*, 1235–1238; c) Z. J. Wang, C. J. Brown, R. G. Bergman, K. N. Raymond, F. D. Toste, *J. Am. Chem. Soc.* **2011**, *133*, 7358–7360; d) M. Otte, P. F. Kuijpers, O. Troeppner, I. Ivanović-Burmazović, J. N. H. Reek, B. De Bruin, *Chem. Eur. J.* **2013**, *19*, 10170–10178; e) S. S. Nurttila, W. Brenner, J. Mosquera, K. M. van Vliet, J. R. Nitschke, J. N. H. Reek, *Chem. Eur. J.* **2019**, *25*, 609–620; f) Y. Ueda, H. Ito, D. Fujita, M. Fujita, *J. Am. Chem. Soc.* **2017**, *139*, 6090–6093.

[3] a) A. B. Grommet, M. Feller, R. Klajn, *Nat. Nanotechnol.* **2020**, *15*, 256–271; b) V. Mouarrawis, R. Plessius, J. I. van der Vlugt, J. N. H. Reek, *Front. Chem.* **2018**, *6*, 623.

[4] a) S. H. A. M. Leenders, R. Gramage-Doria, B. De Bruin, J. N. H. Reek, *Chem. Soc. Rev.* **2015**, *44*, 433–448; b) K. Wang, J. H. Jordan, X. Y. Hu, L. Wang, *Angew. Chem. Int. Ed.* **2020**, *59*, 13712–13721; Angew. Chem. **2020**, 132, 13816–13825.

[5] M. Otte, P. F. Kuijpers, O. Troeppner, I. Ivanović-Burmazović, J. N. H. Reek, B. De Bruin, *Chem. Eur. J.* **2014**, *20*, 4880–4884.

[6] F. J. Rizzuto, L. K. S. von Krbek, J. R. Nitschke, *Nat. Rev. Chem.* **2019**, *3*, 204–222.

[7] a) E. G. Percástegui, J. Mosquera, T. K. Ronson, A. J. Plajer, M. Kieffer, J. R. Nitschke, *Chem. Sci.* **2019**, *10*, 2006–2018; b) A. B. Grommet, J. B. Hoffman, E. G. Percástegui, J. Mosquera, D. J. Howe, J. L. Bolliger, J. R. Nitschke, *J. Am. Chem. Soc.* **2018**, *140*, 14770–14776.

[8] a) Y. Chen, J. V. Ruppel, X. P. Zhang, *J. Am. Chem. Soc.* **2007**, *38*, 2365–2369; b) Y. Chen, K. B. Fields, X. P. Zhang, *J. Am. Chem. Soc.* **2004**, *126*, 14718–14719; c) Y. Chen, X. P. Zhang, *J. Org. Chem.* **2007**, *72*, 5931–5934.

[9] a) M. Tominaga, K. Suzuki, T. Murase, M. Fujita, *J. Am. Chem. Soc.* **2005**, *127*, 11950–11951; b) W. Brenner, T. K. Ronson, J. R. Nitschke, *J. Am. Chem. Soc.* **2017**, *139*, 75–78; c) C. M. Hong, M. Morimoto, E. A. Kapustin, N. Alzakhem, R. G. Bergman, K. N. Raymond, F. D. Toste, *J. Am. Chem. Soc.* **2018**, *140*, 6591–6595; d) Y. Sun, C. Chen, P. J. Stang, *Acc. Chem. Res.* **2019**, *52*, 802–817.

[10] W. Meng, B. Breiner, K. Rissanen, J. D. Thoburn, J. K. Clegg, J. R. Nitschke, *Angew. Chem. Int. Ed.* **2011**, *50*, 3479–3483; *Angew. Chem.* **2011**, *123*, 3541–3545.

[11] A. J. McConnell, C. J. E. Haynes, A. B. Grommet, C. M. Aitchison, J. Guilleme, S. Mikutis, J. R. Nitschke, *J. Am. Chem. Soc.* **2018**, *140*, 16952–16956.

[12] C. Bannwarth, S. Ehlert, S. Grimme, *J. Chem. Theory Comput.* **2019**, *15*, 1652–1671.

[13] F. J. Rizzuto, W. J. Ramsay, J. R. Nitschke, *J. Am. Chem. Soc.* **2018**, *140*, 11502–11509.

[14] L. Huang, Y. Chen, G. Y. Gao, X. P. Zhang, *J. Org. Chem.* **2003**, *68*, 8179–8184.

[15] W. I. Dzik, X. Xu, X. P. Zhang, J. N. H. Reek, B. de Bruin, *J. Am. Chem. Soc.* **2010**, *132*, 10891–10902.

[16] Y. R. Luo, *Comprehensive Handbook of Chemical Bond Energies*, *Vol. 1*, Taylor & Francis, Boca Raton, **2007**, pp-550–560.

[17] A. F. Lago, T. Baer, *J. Phys. Chem. A* **2006**, *110*, 3036–3041.

[18] A. Penoni, R. Wanke, S. Tollari, E. Gallo, D. Musella, F. Ragaini, F. Demartin, S. Cenini, *Eur. J. Inorg. Chem.* **2003**, 1452–1460.

[19] N. R. Forde, L. J. Butler, S. A. Abrash, *J. Chem. Phys.* **1999**, *110*, 8954–8968.

[20] W. I. Dzik, X. Xu, X. P. Zhang, J. N. H. Reek, B. De Bruin, *J. Am. Chem. Soc.* **2010**, *132*, 10891–10902.

[21] A. Chirila, M. B. Brands, B. de Bruin, *J. Catal.* **2018**, *361*, 347–360.

[22] T. Yamada, T. Ikeno, H. Sekino, M. Sato, *Chem. Lett.* **1999**, *28*, 719–720.

[23] T. Ikeno, I. Iwakura, S. Yabushita, T. Yamada, *Org. Lett.* **2002**, *4*, 517–520.

[24] D. Zhang, T. K. Ronson, R. Lavendomme, J. R. Nitschke, *J. Am. Chem. Soc.* **2019**, *141*, 18949–18953.

[25] B. W. Musselman, N. Lehnert, *Chem. Commun.* **2020**, *56*, 14881–14884.

Manuscript received: January 28, 2021
Accepted manuscript online: March 29, 2021
Version of record online: May 3, 2021

